NUMERICAL EVALUATION OF THE CORROSION EFFECTS IN PRESTRESSED CONCRETE BEAMS WITHOUT SHEAR REINFORCEMENT

Structural Concrete
Journal of the fib

NUMERICAL EVALUATION OF THE CORROSION EFFECTS IN PRESTRESSED CONCRETE BEAMS WITHOUT SHEAR REINFORCEMENT

Journal:	*Structural Concrete*
Manuscript ID	suco.201900283.R1
Wiley - Manuscript type:	Technical Paper
Date Submitted by the Author:	n/a

Complete List of Authors:	Belletti, Beatrice; Universita degli Studi di Parma, Department of Engineering and Architecture, DIA Vecchi, Francesca; Università degli Studi di Parma, Department of Engineering and Architecture, DIA Bandini, Cecilia; Università degli Studi di Parma, Department of Engineering and Architecture Andrade, Carmen; International Center for Numerical Methods in Engineering, - Sánchez Montero, Javier ; Instituto de Ciencias de la Construcción Eduardo Torroja, Departamento de Construcción

Subject codes:	corrosion, prestressed concrete, analysis and design methods
Keywords:	prestressed beam, corrosion, PARC_CL 2.1 crack model, non-linear finite element method

Abstract:	Corrosion of prestressed concrete structures causes size reduction of strands, degradation of mechanical properties of steel, cracking of the surrounding concrete and bond decay at steel-to-concrete interface. In this paper, a numerical approach able to take into account all the effects involved in the corrosion process by using non-linear finite element analysis (NLFEA) and membrane or shell elements modelling, is proposed. Two different strategies are adopted to model strands: the smeared and the discrete approaches. The results obtained using these latter strategies are validated by comparing NLFEA results with experimental measurements of a naturally corroded prestressed beam tested at the "Instituto de Ciencias de la Construcción Eduardo Torroja" in Madrid. Finally, pros and cons of the proposed modelling approach are critically analysed, demonstrating that considering the actual spatial corrosion distribution is necessary to predict the position where failure occurs.

NUMERICAL EVALUATION OF THE CORROSION EFFECTS IN PRESTRESSED CONCRETE BEAMS WITHOUT SHEAR REINFORCEMENT

NUMERICAL EVALUATION OF THE CORROSION EFFECTS IN PC BEAMS

Beatrice Belletti*
Associate Professor at DIA, University of Parma
Parco Area delle Scienze 181/A, 43124 Parma, Italy
Tel: +390521905930, Fax: +390521905924
beatrice.belletti@unipr.it

Francesca Vecchi
PhD at DIA, University of Parma
Parco Area delle Scienze 181/A, 43124 Parma, Italy
Tel: +390521905930, Fax: +390521905924
francesca.vecchi@unipr.it

Cecilia Bandini
Master student at DIA, University of Parma
Parco Area delle Scienze 181/A, 43124 Parma, Italy
Tel: +390521905930, Fax: +390521905924
cecilia.bandini@studenti.unipr.it

Carmen Andrade
Visiting Research Professor at International Centre for Numerical Methods in Engineering (CIMNE)
Universitat Politècnica de Catalunya (UPC), Barcelona, Spain
candrade@cimne.upc.edu

Javier Sánchez Montero
PhD at Institute Eduardo Torroja of Construction Sciences
Serrano Galvache, Madrid, Spain
javier.sanchez@csic.es

*Corresponding author.

Abstract

Corrosion of prestressed concrete structures causes size reduction of strands, degradation of mechanical properties of steel, cracking of the surrounding concrete and bond decay at steel-to-concrete interface. In this paper, a numerical approach able to take into account all the effects involved in the corrosion process by using non-linear finite element analysis (NLFEA) and membrane or shell elements modelling, is proposed. Two different strategies are adopted to model strands: the smeared and the discrete approaches. The results obtained using these latter strategies are validated by comparing NLFEA results with experimental measurements of a naturally corroded prestressed beam tested at the "Instituto de Ciencias de la Construcción Eduardo Torroja" in Madrid. Finally, pros and cons of the proposed modelling approach are critically analysed, demonstrating that considering the actual spatial corrosion distribution is necessary to predict the position where failure occurs.

Keywords: prestressed beam, corrosion, PARC_CL 2.1 crack model, non-linear finite element method.

1. Introduction

The corrosion of reinforcing steel in reinforced concrete (RC) and prestressed concrete (PC) structures is one of the most important sources of civil engineering and economic problems in developed countries. Indeed, the corrosion attack of reinforcing steel can determine a safety reduction and a change in failure mechanism, even passing from ductile to brittle, and, in the most extreme cases, can cause the collapse of the structure under live loading. In particular, corrosion of steel in PC structures can lead to more serious structural collapses than in RC structures (Li et al., 2011; ACI 222.2R-01, 2001; Nagi, 1992).

The aggressive environment (chlorides in sea water, higher carbon dioxide concentration, climate change, etc.) is the main cause of corrosion, for both ordinary reinforcing steel and prestressed tendons. Local pitting corrosion or uniform corrosion are respectively caused by chloride attack or carbonation attack. Corroded strands are usually characterised by a reduction in wire cross-section and loss of strength and ductility (Rinaldi et al., 2010; Nürnberger, 2002; Zhao et al., 2012). Furthermore, prestressed concrete structure can experience the stress corrosion cracking (SCC) related to the state of stress in the wires (Vu et al., 2009; Sanchez et al., 2007; Sanchez et al., 2008; Sánchez et al. 2017a) and often associated to hydrogen embrittlement (Elices et al., 2012; Sánchez et al., 2016a; Sánchez et al., 2016b; Sánchez et al., 2017b; Nurnberger, 2002).

Considering concrete-to-steel interface behaviour, corrosion leads cracking and/or spalling of the concrete cover (Molina et al., 1993) which cause bond strength reduction and anchorage failure likelihood (FIB 2000; Coronelli et al., 2009; Morcous et al., 2012; Li & Yuan, 2013). Even if lots of models are proposed in literature to take into account the effect of corrosion on bond stress in normal reinforcement (Blomfors et al., 2018; Schlune, 2006; Coronelli & Gambarova, 2004; Mancini & Tondolo, 2013), few models for strands are available in literature.

Although PC structures have been largely diffused in the last 50 years, above all in infrastructures of strategic importance, as viaducts and bridges, the theme of corrosion of these structural typologies is still under investigation and rigorous guidance is not accepted in spite that European Manuals with some guidance rules have been published more than 20 years ago (CONTECVET IN30902I; DURACRETE). Furthermore, tests on natural corroded beams are rare in literature (Recupero & Spinella, 2019) and often there is no detailed information on the spread of corrosion along the length of the strands. Finally, no data are available in literature concerning the study of corroded prestressed beams without transversal reinforcement, with the exception of papers published by Authors (Saucedo et al., 2019).

In the last past years different authors proposed numerical and analytical approaches for the evaluation of the residual capacity of corroded beams (Recupero et al., 2018; Toongoenthong & Maekawa, 2005-amongst few others). Generally, these models are usually tested on artificially corroded prestressed beams and hypothesize degraded properties evenly distributed.

In this paper a numerical approach for the nonlinear finite element analysis of prestressed corroded beams is proposed. Loss in diameter of the rebar, change in mechanical behaviour of both concrete and strands, reduction in bond between rebar/strand and concrete, and loss in pretension are considered. In particular, two modelling strategies of strands are adopted in order to understand how much the bond affects the result: the smeared and discrete approach. Both numerical approaches are validated by means of the comparison with experimental results of the VIGA 470 beam tested at the "Instituto de Ciencias de la Construcción Eduardo Torroja" in Madrid (Saucedo et al., 2019). The VIGA 470 is one of 14 naturally corroded prestressed beams coming from a natural gas power station and characterised by non-uniform corrosion (pitting) induced by chlorides. The numerical analyses are conducted using the PARC_CL 2.1 crack model developed at the University of Parma (Belletti et al., 2017a; Belletti et al., 2017a; Belletti et al., 2018) considering the spatial distribution of the corrosion pattern provided by experimental evidences.

Aims of this study is to understand how corrosion influences the failure mode of prestressed beams and which effects have to be considered to catch the real failure modes and the ultimate capacity of corroded beams using nonlinear finite element analysis (NLFEA).

2. Experimental Test

Fourteen naturally corroded PC beams from the refrigeration tower of a thermal power plant have been tested at the "Instituto de Ciencias de la Construcción Eduardo Torroja" in Madrid. The refrigeration in the thermal power plant has been made with seawater, causing chlorides attack of PC beams. The corroded beams showed heavy damage in the cover near the supports and relevant cracks along the surface due to corrosion. In this paper, only the VIGA 470 beam has been presented and analysed.

The VIGA 470 beam had a total length of 5440 mm, a depth of 300 mm and a width of 150 mm, Figure 1. The beam was characterised by 2 seven wire prestressed strands with a nominal diameter of 1/2 in (12.5 mm), located at the bottom. The value of the pretension applied to the strands, σ_p, was equal to 1408 MPa. The top of the beam was reinforced with 2ϕ5 mm. The beam was without shear reinforcement. The mechanical properties of concrete and steel are summarized respectively in Table 1 and Table2.

Visual inspection was performed to identify and quantify the damage in the beam in terms of presence of cracks and spalling of concrete cover, highlighting the presence of an extended splitting crack in correspondence of the strands and cover expulsion in the left corner, Figure 2.

Subsequently, a three-point bending test was performed on the VIGA 470 beam, as shown in Figure 3. The support plates allowed the section rotation during the test. The distance between supports was equal to 4700 mm. The distance between the right support and the right corner was equal to 200 mm. The distance between the left support and the left corner was equal to 540 mm, obtaining a distance between the support and the damaged zone equal to 200 mm, Figure 2. The load was applied gradually till failure using a manually controlled hydraulic jack directly on the load plate. The displacements were measured under the load application point.

In order to analyse the corrosion distribution along the length of the beam, after the test the concrete cover was removed and the strands were extracted. From the visual inspection five levels of corrosion were considered: not corroded (NC), localized pits (LP), high-density pits (HDP), uniform/generalized corrosion (UC), high corrosion (HC), as summarized in Table 3. For each level of corrosion, a sample was selected and measured. In particular, each sample strand was separated into wires and cleaned from the rust using a cleaning solution (which does not affect the parent metal) and the tank instrument with ultrasound energy shown in Figure 4. After the cleaning procedure, the samples were weighed and measured in terms of length, obtaining the mean values reported in Table 4. Finally, it was possible to obtain the equivalent remaining average area of the strands, Table 4. Subsequently, each strand was divided into 500 mm long pieces which were classified according to the detected level of corrosion defined in Table 4. By means of this procedure the corrosion distribution along both the strands of VIGA 470 beam was defined, Figure 5. Following this procedure, it was obtained that the highest level of corrosion was located in correspondence of the pre-existing splitting crack and the expulsion of concrete cover, as shown in Figure 5.

3. Numerical model

Literature is lacking of experimental tests on PC beams, in particular without transversal reinforcement. There is also lacking of models about the deterioration of materials induced by corrosion of strands. For these reasons, a first approach to model corrosion effects in PC beams using NLFEA is presented. To this aim, the response of one corroded beam, the VIGA 470, has been predicted through non-linear numerical analyses using Abaqus code and PARC_CL 2.1 crack model (Belletti et al., 2017). In order to consider the effects induced by corrosion, the damage model proposed by Lu, Li & Zhao (2016) for the mechanical behaviour of corroded prestressed strands has been used. Furthermore, two different approaches are adopted to evaluate the effect of bond deterioration on the global behaviour of the beam. In particular, the first approach considers prestressed strands as smeared in the concrete elements assuming perfect bond behaviour between strands and concrete; on the contrary, in the second approach the prestressed strands are modelled in a discrete way, considering the corroded bond-slip relationship proposed by Wang et al. (2017).

Finally, in order to be able to better understand the effect of non-uniform corrosion on the local and global behaviour of the beam, the VIGA 470 is modelled also considering uncorroded properties.

3.1. PARC_CL 2.1 crack model

The PARC_CL 2.1 crack model is a new release of previous versions described in detail in Belletti et al. (2017a) and successfully applied to the analysis of RC structures subjected to monotonic, cyclic and dynamic loading. The proposed PARC_CL 2.1 model is based on a total strain fixed crack approach, in which at each integration point two reference systems are defined: the local *x,y*-coordinate system and the *1,2*-coordinate system along the principal stress directions. The angle between the *1*-direction and the *x*-direction is denoted as ψ, whereas θ_i is the angle between the direction of the *i*th order of bars and the *x*-direction; $\alpha_i = \theta_i - \psi$ is the direction of the *i*th bars with respect to direction 1. The element begins to crack when the principal tensile strain in concrete exceeds the concrete tensile limit strain $\varepsilon_{t,cr}$. Since the formation of the first crack, the *1,2*-coordinate system remains fixed, Figure 6(a) at the integration point. The cracking is assumed as being uniform, the orientation of the cracks remains fixed upon further loading and the crack spacing a_m is assumed to be constant. The main quantities governing the problem are the crack opening w and the crack slip v, Figure 6(b). For further details, the reader can therefore refer to Belletti et al. (2017a).

3.2. Non-linear finite element model of VIGA 470 beam

3.2.1. Element type and finite element mesh

NLFE analyses have been carried out using 8-node membrane elements with reduced integration scheme (defined M3D8R in Abaqus 2016). The average mesh size was equal to 34x20mm. Concrete and normal reinforcement have been modelled using the PARC_CL 2.1 crack model. In particular, the normal reinforcement (2ϕ5 mm) has been assumed smeared in the concrete element, adopting the Menegotto & Pinto 1998 law, implemented in the PARC_CL 2.1 crack model.

VIGA 470 beam has been modelled considering the spatial distribution of the corrosion pattern provided by experimental evidences and shown in Figure 5. Since a 2D modelling approach has been carried out, the two strands have been modelled using area, stress and strength values calculated as the average value of the two strands. Following the corrosion pattern of VIGA 470 beam shown in Figure 5, element sets are defined. More specifically, the cross-sectional area of each set has been considered as a sum of the areas of the two single tendons referred to their corrosion degree. Combining the value of the cross-sectional area it is possible to obtain the average value to use for the numerical model. For example, the set 4 composed of a tendon with the "Uniform Corrosion" level and the "High-Density Pits" level, has been characterized by a total cross-sectional area equal to 82.94+87.83=170.765 mm^2. Following this procedure, it has been possible to associate to each set the corroded properties.

The NLFE analyses have been carried out in displacement control using implicit solution method and Newton-Raphson convergence criterion. Support and loading plates have been modelled assuming a linear elastic behavior. Interface elements, having no-tension behavior, have been used between steel plates and the beam at the supports and loading positions. The mechanical features of the interface elements are summarized in Table 5. The translations along the *x* and *y*-direction at a single node of the left steel support plate have been constrained as well as the translation along the *y*-direction at the right steel support plate.

3.2.2. Concrete model and parameters

The compressive strength of the damaged concrete, f'_c, has been decreased according to the formulation proposed by Coronelli & Gambarova 2004 for normal reinforcement, Equation (1):

$$f'_c = \frac{f_c}{1 + K^{\varepsilon_1}/_{\varepsilon_{c0}}} \quad (1)$$

where f_c is the compressive strength of undamaged concrete; K is a coefficient related to the bar roughness and diameter; ε_1 is the average strain in the cracked concrete at right angles to the direction of the applied compression; ε_{c0} is the strain at the peak compressive stress f_c. The strain ε_1 is evaluated using Equation (2):

$$\varepsilon_1 = (b_f - b_0)/b_0 \quad (2)$$

where b_0 is the section width in the uncorroded state and b_f is the beam width increased by corrosion cracking, approximated as in Equation (3):

$$b_f = b_0 + n_{bars} \cdot w_{cr} \quad (3)$$

where n_{bars} is the number of the bars in the top layer (compressed bars) and w_{cr} is the total crack width for a given corrosion level X. The value of w_{cr}, according to Coronelli & Gambarova (2004), is evaluated using the relation proposed by Molina et al. (1993), as indicated in Equation (4):

$$w_{cr} = \sum_i u_{i\,corr} = 2\pi(v_{rs} - 1) \cdot X \quad (4)$$

where v_{rs} is the ratio of volumetric expansion of the oxides with respect to the uncorroded material; X is the depth of the corrosion attack and $u_{i\,corr}$ is the opening of each single corrosion crack. The value v_{rs} is taken equal to 2, according to Molina et al. (1993). Finally, the value of the penetration attack X is evaluated according to Equation (5), as proposed by Zandi Hanjari et al. (2011) and Molina et al. (1993).

$$X = \frac{\phi - \phi'}{2} \quad (5)$$

where ϕ' is the corroded diameter.

The result is a reduction of about 75% of the concrete strength in the zone of the beam affected by splitting (shown in Figure 2). As consequence, also the tensile strength of concrete has been reduced according to the compressive strength of the damaged concrete, f_c'. Adopted values for mechanical properties of damaged concrete are reported in Table 6 and Figure 7. In order to take into account this effect in NLFEA, an elements set (shown in ocher color in Figure 9 and Figure 10) with reduced mechanical properties of concrete has been added in correspondence of the splitting crack. Furthermore, in the zone of the beam affected by splitting (shown in Figure 2), the aggregate interlock has been reduced of 70% in order to consider the effect of corrosion on concrete resistance.

3.2.3. Steel model and parameters

When corrosion occurs, the mechanical behavior of the steel changes. In particular, in prestressed strands, decreases of wire sections due to corrosion causes high stresses triggering sudden structural collapse (ACI 222. 2R-01, 2001; Bergsma, Boon & Etienne, 1977). In previous studies the properties of the corroded reinforcements were studied and it was found out that the stress-strain curve of the corroded steel is affected by the corrosion degree. The ductility and the strength of the residual section decrease. This is recognized in Lu, Li & Zhao (2016) paper who proposed a damage model for failure mechanism of corroded prestressed strands that has been adopted in this paper. In Lu, Li & Zhao (2016) damage model, the following mechanical properties are dependent on corrosion level: the elastic modulus, E_s', Equation (6), the ultimate strength of strands, f_u' (due to the stress concentration caused by pitting corrosion and/or eccentric tension due to asymmetric corrosion distribution), Equation (7), and the ultimate strain, ε_u', Equation (8). Furthermore, Lu, Li & Zhao (2016) observed that when the corrosion degree is larger than 8% the steel loses the yielding plateau and the strain hardening region.

$$D(E,t) = E_s'/E_s \qquad D(E,t) = 1 - 1.8 \cdot f(D) \qquad (6)$$

$$D(f,t) = f_u'/f_u \qquad D(f,t) = 1 - 2.8 \cdot f(D) \qquad (7)$$

$$D(\varepsilon,t) = \varepsilon_u'/\varepsilon_u \qquad D(\varepsilon,t) = 0.1 + 0.9e^{[-20 f(D)]} \qquad (8)$$

In this study, $f(D)=D(t)$, where $D(t)$ is the area damage factor defined in Equation (9):

$$D(t) = (A - A')/A \qquad (9)$$

where A is the uncorroded area equal to 93 mm^2, while A' is the corroded area, Table 4.

Finally, according to experimental evidences, Lu, Li & Zhao (2016) proposed constitutive laws for corroded strands in function of the average corrosion degree, η_s, defined in Equation (10):

$$\eta_s = [(A - A')/A] * 100\% \tag{10}$$

When strands are characterized by average corrosion degree, η_s, less than the critical value defined η_{scr}=8%, the constitutive law is defined by Equation (11). Instead, when the average corrosion degree η_s is greater than η_{scr} the hardening plateau disappears and the constitutive law is characterized by the elastic branch as in Equation (12).

$$\eta_s \le \eta_{scr} \quad \sigma(\varepsilon) = \begin{cases} E_s' \cdot \varepsilon & \varepsilon \le \varepsilon_y' = 0.85 f_u' / E_s' \\ 0.85 \cdot f_u' + \dfrac{0.15 \cdot f_u'}{\varepsilon_u' - \varepsilon_y'} \{\varepsilon - \varepsilon_y'\} & \varepsilon_y' < \varepsilon \le \varepsilon_u' \end{cases} \tag{11}$$

$$\eta_s > \eta_{scr} \quad \sigma(\varepsilon) = E_s' \cdot \varepsilon \tag{12}$$

Finally, the obtained mechanical properties and the constitutive models for corroded strands of VIGA 470 beam are shown respectively in Table 7 and Figure 8 in function of the corrosion degree. Since a 2D modelling approach has been carried out, when the sets defined in Figure 5 are characterized by different corrosion levels, average mechanical properties have been adopted.

3.2.3.1. Smeared approach for strands

The smeared approach hypothesis considers a perfect bond condition between concrete and strands. Prestressing strands have been modelled using rebar layers, embedded in the ''host'' concrete shell elements, Figure 9.

3.2.3.2. Discrete approach for strands

In the discrete approach beam elements with 3-nodes and 2 integration points (defined B32 in Abaqus, 2016) have been adopted to model the strands, Figure 10. In order to consider the interaction between concrete and steel, the beam elements are connected to the membrane elements by means of two sets of un-coupled springs. The first spring set defines the radial behavior, while the second spring set defines the bond-slip relation, Figure 10.

Differently to the smeared approach, in the discrete one a bond-slip relationship has been associated to springs element. In particular, since the Model Code 2010 (*fib* 2013) bond-slip relationship is not suitable for strands, the model proposed by Wang et al. (2017) has been assumed for modeling the bond-slip relationship. The model by Wang et al. (2017) is a modification of the Model Code 2010 (*fib* 2013) relationship for splitting failure of uncorroded elements with confining stirrups, Equation (13):

$$\tau = \begin{cases} \tau_{max}\left(\frac{s}{s_2}\right)^{\alpha} & 0 \leq s < s_1 \\ \tau_{max} - (\tau_{max} - \tau_f)\left(\frac{s - s_2}{s_3 - s_2}\right) & s_2 \leq s < s_3 \\ \tau_f = 0.4 \cdot \tau_{max} & s_3 \leq s \end{cases} \quad (13)$$

The maximum value of bond stress τ_{max} is equal to $1.25\sqrt{f_c}$; $s_2 = 3$ mm, s_3 is half of the distance between concrete gear and the adjacent wires (12 mm according to the authors), α is a constant equal to 0.4 and τ_f is a constant residual strength. Since the VIGA 470 was without stirrups, in this paper the residual strength, τ_f, has been assumed to be equal to zero. Furthermore, an $R(\eta_s)$ factor (Wang et al., 2017) has been used to calculate the reduction of maximum bond stress due to corrosion, τ'_{max}, according to Equation (14)-(15):

$$R(\eta_s) = \begin{cases} 1{,}0 & \eta_s \leq 6\% \\ 2{,}03e^{-0{,}118 \cdot \eta_s} & \eta_s > 6\% \end{cases} \quad (14)$$

$$\tau'_{max}(s) = R(\eta_s) \cdot \tau_{max} \quad (15)$$

The obtained values of $R(\eta_s)$ factor for different levels of corrosion are summarized in Table 7. As shown in Figure 11(a), for low value of the average corrosion degree η_s the bond-slip relationship does not change and is equal to the case of uncorroded strand. Once the value of the maximum bond stress τ'_{max}, for each corrosion level, is defined, the bond-slip relationship, expressed in Equation (13), is assigned to spring elements.

In correspondence of the splitting crack it is reasonable to consider that splitting failure is occurring. For this reason, the local bond stress-slip relationship in correspondence of the splitting crack (i.e. springs placed in correspondence of elements in ocher color in Figure 10) can be approximated by shifting the reference curve in the slip direction, as shown in Figure 11 (b).

3.2.4. Prestressing force and losses

The main prestress losses considered in the model are: elastic shortening of the concrete, relaxation of strands and concrete time dependent losses due to creep and shrinkage. The elastic shortening is calculated during the analysis by the software Abaqus. The relaxation loss, $\Delta\sigma_{pr}$, is determined according to EN 1992-1-1, 2002 assuming the case of ordinary prestressing and low relaxation strands (Class 2). The obtained loss value due to the relaxation of strands at time of 10 years (beam age), is equal to 30.5 MPa. Shrinkage and creep effects have been calculated according to Model Code 2010 (*fib* 2013) considering a beam age equal to 10 years, obtaining respectively strain values equal to ε_{sh}=6.28e^{-4} and ε_{creep}=2.64e^{-4}. The shrinkage effect in PARC_CL 2.1 model has been applied considering an average deformation, without resolving the solution of thermo-hygrometric problems and neglecting temporal and spatial evolution of the phenomenon (Belletti et al., 2018). The creep effects have been applied by imposing a temperature gradient to the nodes of the mesh.

The final prestress value, σ_p, for uncorroded strands is equal to 1377 MPa and it has been applied gradually over the transmission length, l_{pt} according to EN 1992-1-1, 2002, Eq.(16).

$$l_{pt} = \alpha_1 \cdot \alpha_2 \cdot \phi \cdot \sigma_{pm0}/f_{bpt} \tag{16}$$

where α_1=1 for gradual release, α_2=0.19 for 7-wire strands, ϕ is the nominal diameter of tendon and σ_{pm0} is the strand stress just after the release. At release of strands the prestress may be assumed to be transferred to the concrete by a constant bond stress, f_{bpt}, defined in Eq.(17):

$$f_{bpt} = \eta_{p1} \cdot \eta_1 \cdot f_{ctd}(t) \tag{17}$$

where η_{p1} = 3.2 for 7-wire strands, η_1=1 for good bond conditions. $f_{ctd}(t)$ is the design tensile value of strength at time of release, as expressed in Equation (18):

$$f_{ctd}(t) = \alpha_{ct} \cdot 0.7 \cdot f_{ctm}(t)/\gamma_c \tag{18}$$

where the coefficient α_{ct} is taken equal to 1 and γ_c is the partial safety factor for concrete is taken equal to 1. Finally, the transfer length l_{pt} is equal to 415 mm.

Corrosion affects also the pretension in the strands (Rashetnia et al., 2018; Dasar et al., 2016), even if a direct correlation between the corrosion degree and loss in pretension caused by corrosion has not yet been found. In this paper, the loss in pretension due to corrosion is estimated by using Equation (19):

$$\sigma'_p = D(f,t) \cdot \sigma_p \tag{19}$$

where σ'_p is the reduced pretension due to corrosion, σ_p is the pretension for uncorroded strand and $D(f,t)$ is defined in Equation (7). The applied pretension in function of the corrosion levels is shown in Figure 9.

Prestressing stress has been defined as a given initial condition together with dead load. The result of this first step is a self-equilibrating stress state. Therefore, the prestressing force does not remain constant during all the analysis steps, but it changes following the development of the cracking pattern up to failure.

3.3. Comparison between NLFE analyses and experimental results

During the experimental test, the beam showed a sudden brittle failure in correspondence of a load equal to 26 kN, with concrete cover expulsion in correspondence of the splitting crack, Figure 12(a). The beam at the end of the test showed a shear and bond failure, according to the definition expressed in the CONTECVET [CONTECVET IN30902I, (2001), Figure 12(b). In correspondence of the concrete cover expulsion the strands were highly corroded with some wires broken, Figure 12(c-d). The load-displacement curve is characterized only by the elastic part, losing any ductile behaviour, Figure 13.

Figure 14 and Figure 15 show the numerical results obtained using the smeared and the discrete approach respectively. Both the models demonstrate to be able to catch with good approximation the ultimate resistance of the beam. Since the NLFEA have been carried out in displacement control, the numerical ductility results higher than the ductility measured during experimental test carried out in load control.

The failure mode obtained using both the approaches is governed by high crack opening width values, Figure 14(a) and Figure 15(a), without crushing of concrete, Figure 14(b) and Figure 15(b). A single crack was formed, characterized by a horizontal part and an inclined part. The formed crack is due to a biaxial state governed by tensile stresses induced by bending and shear stresses induced by shear. The layer of concrete plain elements above the strands is characterized by a different stiffness and strength that increases tangential shear stresses in concrete, causing the formation of the horizontal crack where the mechanical properties of concrete have been degraded due to strands corrosion effects. In Figure 14(c) and Figure 15(c), the strands stresses obtained by NLFEA along the beam are shown for smeared and discrete approach respectively and compared with the yielding stresses associated to each corrosion level: in both the cases, the strands have not reached the yielding stress. In the smeared approach the NLFEA stopped due to the reaching of high value of crack openings in correspondence of the splitting crack, as shown in Figure 14. In the discrete approach, in addition to high crack opening values, the NLFEA shows the reaching of the maximum bond stress in correspondence of the splitting crack, Figure 15(d).

3.4. Comparison between NLFEA capacity prediction of uncorroded and corroded beam

In order to better appreciate the effect induced by the proposed corrosion modelling, the VIGA 470 beam is also modelled using the undamaged mechanical properties of concrete (Figure 7), uncorroded properties for strands (Figure 8) and applying a prestress value, σ_p , equal to 1377 MPa (Figure 9).

The uncorroded beam was modelled using the smeared and discrete approach and in both cases it shows flexural cracks typical of bending failure mode, Figure 16. The failure is due to concrete crushing in correspondence of the loading plate, as shown in Figure 17, where the black elements have reached the ultimate compressive strain according to Figure 7. At failure the strands at mid-span have overcome the yield stress (equal to 1580 MPa) (Figure 18).

Finally, the uncorroded beam exhibits a ductile behavior reaching a final displacement of about 29 mm and an ultimate resistance of 57 kN, as shown in Figure 19. In this case, the response of the uncorroded beam is characterized by a resistance and ductility capacity respectively equal to two and five times the resistance and ductility capacity of the corroded beam. Comparing the crack patterns of Figure 16 with Figure 14(a) and Figure 15(a) it is possible to conclude that the modelling of the actual spatial pits distribution and the corrosion levels along the beam permits to obtain a more accurate prediction of the position where failure occurs.

4. Conclusions

In this paper, a numerical approach able to take into account the effect of non-uniform corrosion in prestressed elements has been proposed. Aim of the work is to develop a suitable methodology for modelling the behaviour of corroded PC structures able to take into account the large number of the parameters that come into play. Two modelling strategies are proposed (smeared considering perfect bond between concrete and strands and discrete considering deteriorated bond-slip relationship) and are applied to a naturally corroded prestressed beam. The main conclusions are reported in the following:

- NLFE analyses results obtained are able to catch with good approximation the ultimate displacement and the ultimate load, highlighting a brittle behaviour and the complete loss of ductility at failure.
- The approaches are proposed to model the interaction between concrete and strands: the smeared considering perfect bond and the discrete considering deteriorated bond-slip relationship. Both the approaches are able to predict with good approximation the load-displacement curve and the localization of the splitting crack found in the experimental test.
- Considering non-uniform corrosion distribution permits to obtain a more realistic crack pattern.
- The comparison between the results obtained for the uncorroded beam and the corroded beam proves the potentiality of the proposed modelling approach in predicting the ultimate load and ultimate displacement of the VIGA 470 beam, as well as the capacity to catch the experimental failure mode.
- Future developments will be aimed at investigating in more detail the collapse mechanisms of PC structures and evaluate in which cases the discrete approach is preferable and necessary. The proposed model will be applied to a large set of prestressed concrete beams in order to validate the procedure. Furthermore, the role of the bond at the serviceability limit states will be investigated in order to be able to provide a useful tool for the remaining service life prediction of existing structures.

Acknowledgements

The authors wish to acknowledge the structural lab of the Institute Eduardo Torroja CSIC (headed by C. Lopez) and to J. Rodriguez for the design of the testing, to L. Saucedo and S. Zambonini for its performance.

The financial support from the Italian Ministry of Education, University and Research (PRIN Grant 2015HZ24KH—"Failure mechanisms caused by corrosive degrade and by lack of constructive details in the existing structures in reinforced concrete") is gratefully acknowledged.

References

Abaqus 6.12 (2012). *User's and theory manuals*; 2012 <http://www.3ds.com/> [1 June 2016].

ACI 222.2R-01 (2001). Corrosion of prestressing steels – *ACI Committee 222*.

Belletti, B., Scolari, M., & Vecchi, F. (2017a). PARC_CL 2.0 crack model for NLFEA of reinforced concrete structures under cyclic loadings. *Comput Struct*, *191*(2017), 165-179. https://doi.org/10.1016/j.compstruc.2017.06.008

Belletti, B., Stocchi, A., Scolari, M., & Vecchi, F. (2017b). Validation of the PARC_CL 2.0 crack model for the assessment of the nonlinear behaviour of RC structures subjected to seismic action: SMART 2013 shaking table test simulation. *Engineering Structures*, *150*(2017), 759-773. https://doi.org/10.1016/j.engstruct.2017.07.058

Belletti, B., Muttoni, A., Vecchi, F., & Ravasini, S. (2018). Parametric analysis on punching shear resistance of reinforced concrete continuous slabs. *Magazine of Concrete Research*, DOI: 10.1680/jmacr.18.00123

Bergsma, F., Boon, J.W., & Etienne, C.F. (1977). Endurance tests for the determining the susceptibility of prestressing steel to hydrogen embrittlement. *HERON*, *22*(1), 46-71.

Blomfors, M., Zandi, K., Lundgren, K., & Coronelli, D. (2018). Engineering bond model for corroded reinforcement. *Engineering Structures, 156*(2018), 394-410. https://doi.org/10.1016/j.engstruct.2017.11.030

CONTECVET IN30902I, (2001). *A validated user's manual for assessing the residual life of concrete structures, DG Enterprise, CEC*, (The manual for assessing reinforced structures affected by reinforcement corrosion can be seen at the web sites of IETcc (www.ietcc.csic.es) and GEOCISA (www.geocisa.es)).

Coronelli, D., & Gambarova, P. (2004). Structural Assessment of Corroded Reinforced Concrete Beams: Modeling Guidelines. *ASCE-J StructEng,130*(8), 1214-24.

Coronelli, D., Castel, A., François, R., & Cleland, D. (2009). Modelling the response of prestressed beams with corroded reinforcement. *European Journal of Environmental and Civil Engineering*, *13*(6), 653-669. https://doi.org/10.1080/19648189.2009.9693144

Dasar, A., Irmawaty, R., Hamada, H., Sagawa, Y., & Yamamoto, D. (2016). Prestress Loss and Bending Capacity of Pre-cracked 40 Years-Old PC Beams Exposed to Marine Environment. *MATEC Web of Conferences,* The 3rd International Conference on Civil and Environmental Engineering for Sustainability *(IConCEES 2015), 47*, 02008.

DURACRETE. *Probabilistic performance based on durability design of concrete structures.* EU-Brite EuRam Project BE95-1347. A number of reports available from CUR Centre for Civil Engineering Research and Codes, Gouda, The Netherlands.

Elices, M., Valiente, A., Caballero, L., Iordachescu, M., Fullea, J., Sánchez-Montero, J., & López-Serrano, V. (2012). Failure analysis of prestressed anchor bars. *Engineering Failure Analysis, 24*(0), 57-66. https://doi.org/10.1016/j.engfailanal.2012.03.007

EN 1992-1-1, 2002. *Eurocode 2: Design of concrete structures*. - Part1-1: General rules and rules 516 for buildings; 2004.

Federation International du Beton FIB. (2000). *Bond of reinforcement in concrete. State of the Art Report—Bulletin 10*—Task Group Bond Models, Lausanne (CH), 427.

fib – International federation for structural concrete. fib model code for concrete structures 2010. 431 Ernst & Sohn; 2013; 434 p.

Li, F., & Yuan, Y. (2013). Effects of corrosion on bond behavior between steel strand and concrete. *Construction and Building Materials*, *38*(2013), 413-422. https://doi.org/10.1016/j.conbuildmat.2012.08.008

Li, F., Yuan, Y., Li, Chun-Qing (2011). Corrosion propagation of prestressing steel strands in concrete subject to chloride attack. *Construction and Building Materials, 25*(2011), 3878-3885. https://doi.org/10.1016/j.conbuildmat.2011.04.011

Lu, Z.-H., Li, F., & Zhao, Y.-G. (2016). An investigation of degradation of mechanical behaviour of prestressing strands subjected to chloride attacking. *5th International Conference on Durability of Concrete Structures*, Shenzhen University, China.

Mancini G., Tondolo F. (2013). Effect of bond degradation due to corrosion – a literature survey. *Structural Concrete, 15 (3).* https://doi.org/10.1002/suco.201300009

Menegotto, M, & Pinto, P.E. (1998). Method of analysis for cyclically loaded R.C. plane frames including changes in geometry and non-elastic behaviour of elements under combined normal force and bending. *Symposium* *on the Resistance and Ultimate Deformability of Structures Acted on by Well Defined Repeated Loads*. Lisbon (Portugal): International Association for Bridge and Structural Engineering (ABSE); 1973.

Molina, F.J., Alonso, C., & Andrade, C. (1993). Cover cracking as a function of rebar corrosion. II: Numerical model. *Mater. Struct.*, *26*, 532–548.

Morcous, G., Hatami, A., Maguire, M., Hanna, K., & Tadros M.K. (2012). Mechanical and Bond Properties of 18-mm- (0.7-in.-) Diameter Prestressing Strands. *J. Mater. Civ. Eng.*, *24*(2012), 735-744.

Nagi, W. (1992). Corrosion of prestressed reinforcing steel in concrete bridges: state of the art. [*ACI-SP 151-2*].

Nürnberger, U. (2002). *Corrosion induced failures of prestressing steel.* Otto-Graf J 2002;12.

Rashetnia, R., Ghasemzadeh, F., Hallaji, M., & Pour-Ghaz, M. (2018). Quantifying prestressing force loss due to corrosion from dynamic structural response. *Journal of Sound and Vibration, 433*(2018), 129-137. https://doi.org/10.1016/j.jsv.2018.07.012

Rinaldi, Z., Imperatore, S., & Valente, C. (2010). Experimental evaluation of the flexural behavior of corroded P/C beams. *Construction and Building Materials, 24*(2010), 2267-2278. https://doi.org/10.1016/j.conbuildmat.2010.04.029

Recupero, A., Spinella, N., & Tondolo, F. (2018). Experimental tests on corroded prestressed concrete beams subjected to transverse load. *Structural Concrete*. https://doi.org/10.1002/suco.201900242

Recupero, A., Spinella, N., & Tondolo, F. (2018). A model for the analysis of ultimate capacity of RC and PC corroded beams. *Advances in Civil Engineering*, *2018*, Article ID 8697109, 13 pages. https://doi.org/10.1155/2018/8697109

Sanchez, J., Fullea, J., Andrade, C., & Alonso, C. (2007). Stress corrosion cracking mechanism of prestressing steels in bicarbonate solutions. *Corrosion Science, 49*(11), 4069-4080. https://doi.org/10.1016/j.corsci.2007.05.025

Sanchez, J., Fullea, J., & Andrade, C. (2008). Fracture toughness variation induced by stress corrosion cracking of prestressing steels. *Materials and Corrosion*, *59*(2), 139-143. https://doi.org/10.1002/maco.200804171

Sanchez, J., Lee, S.F., Martin-Rengel, M.A., Fullea, J., Andrade, C., & Ruiz-Hervías, J. (2016a). Measurement of hydrogen and embrittlement of high strength steels. *Engineering Failure Analysis, 59*, 467-477. https://doi.org/10.1016/j.engfailanal.2015.11.001

Sánchez, J., Ridruejo, Á., Muñoz, E., Andrade, C., Fullea, J., & de Andres, P. (2016b). Cálculo de la velocidad de propagación de la fisura debido a fragilización por hidrógeno. *Hormigón y Acero, 67*(280), 325-332.

https://doi.org/10.1016/j.hya.2016.01.002

Sanchez, J., Fullea, J., Andrade, C. (2017a). Corrosion-induced brittle failure in reinforcing steel. *Theoretical and Applied Fracture Mechanics, 92*(Supplement C), 229-232. https://doi.org/10.1016/j.tafmec.2017.08.006

Sanchez, J., Fullea, J., Andrade, C. (2017b). Fracto-surface mobility mechanism in high-strength steel wires. *Engineering Fracture Mechanics, 186*(Supplement C), 410-422. https://doi.org/10.1016/j.engfracmech.2017.11.003

Saucedo, L., Andrade, C., Belletti, B., Vecchi, F., Zambonini, S., Santiago, J.R., & Montero, J.S. (2019). Corrosion effects in prestressed concrete beams: Experimental test and non-linear finite element analysis. *Proceedings of the fib Symposium 2019: Concrete - Innovations in Materials, Design and Structures 2019*, Krakow, Poland, 27-29 May 2019, 905-912.

Schlune, H. (2006). Master Thesis, *Bond of corroded reinforcement, Analytical description of the bond-slip response.* Chalmers University of Technology.

Toongoenthong, K., & Maekawa, K. (2005). Multi-mechanical approach to structural performance assessment of corroded RC members in shear. *Journal of Advanced Concrete Technology*, *3*(1), 107–122.

Vu, N.A., Castel, A., & Francois, R. (2009). Effect of stress corrosion cracking on stress–strain response of steel wires used in prestressed concrete beams. *Corrosion Science, 51*(2009), 1453-1459. https://doi.org/10.1016/j.corsci.2009.03.033

Wang, L.A.M., Zhang, X., Zhang, J., Yi, J., & Liu, Y. (2017). Simplified Model for Corrosion-Induced Bond Degradation between Steel Strand and Concrete. *Journal of Materials in Civil Engineering, 29*(4):04016257-1:11.

Zandi Hanjari, K., Kettil, P., & Lundgren, K. (2011). Analysis of Mechanical Behavior of Corroded Reinforced Concrete Structures. *ACI Structural Journal*, 108(5), 532-541.

Zhao, Y., Yu, J., Hu, B., & Jin, W. (2012). Crack shape and rust distribution in corrosion-induced cracking concrete. *Corros. Sci., 55*, 385–393. https://doi.org/10.1016/j.corsci.2011.11.002

LIST OF FIGURES

Figure 1. Longitudinal section and cross section of VIGA 470 beam [mm].

Figure 2. VIGA 470 beam: quantified damage by visual inspection.

Figure 3. Test setup of VIGA 470 beam.

Figure 4. Ultrasound accelerating reaction instrument.

Figure 5. VIGA 470: Correlation between visual inspection and corrosion pattern of the strands.

Figure 6. PARC_CL 2.1 crack model: (a) RC membrane element subject to plane stress state, (b) crack parameters.

Figure 7. Smeared model and pretension applied to prestressed steel.

Figure 8. Discrete model and connection between membrane elements and beam elements.

Figure 9. Concrete damage model in compression.

Figure 10. Constitutive model for corroded strands.

Figure 11. Bond-Slip relationship for splitting failure: (a) deterioration of bond according to Wang et al. (2017) and (b) bond-slip relationship adopted in NLFEA in correspondence of the splitting crack.

Figure 12. Viga 470 beam at failure: (a) front side, (b) detail of the crack in the back side, (c) and (d) details of corroded strands in correspondence of the concrete cover expulsion.

Figure 13. Comparison between experimental and numerical results.

Figure 14. NLFE results at the end of the analysis obtained using the smeared approach: (a) crack width, *w*, (b) concrete strain and (c) strands stresses.

Figure 15. NLFE results at the end of the analysis obtained using the discrete approach: (a) crack width, *w*, (b) concrete strain, (c) strands stresses and (d) bond stresses.

Figure 16. Crack pattern at failure of the uncorroded beam obtained by NLFE analysis: (a) smeared approach and (b) discrete approach.

Figure 17. Concrete strain, ε_c, at failure obtained by NLFE analysis of the uncorroded beam: (a) smeared approach and (b) discrete approach.

Figure 18. Strands stress, f_p, at failure obtained by NLFE analysis of the uncorroded beam: (a) smeared approach and (b) discrete approach.

Figure 19. Comparison between experimental and numerical results using uncorroded properties.

Table 1. Mechanical properties of concrete.

f_c	f_{ct}	E_c
43.65MPa	3.25MPa	35137MPa

Table 2. Mechanical properties of steel.

Reinforcement (2ϕ5)				**Wire (2ϕ1/2)**			
A_s **[mm²]**	E_s **[MPa]**	f_y **[MPa]**	f_u **[MPa]**	A_s **[mm²]**	E_s **[MPa]**	$f_{p0,1k}$ **[MPa]**	f_{ptk} **[MPa]**
39.25	200000MPa	435MPa	500MPa	186mm²	195000MPa	1580MPa	1860MPa

Table 3. Legend and abbreviation of corrosion levels.

CORROSION LEVELS	**ABBREVIATION**	**SAMPLES**
Not corroded	**NC**	
Localized Pits	**LP**	
High-DensityPits	**HDP**	
Uniform corrosion	**UC**	
High Corrosion	**HC**	

Table 4. Average mass loss, length and area of different levels of corrosion of strands.

LEVEL OF CORROSION		**Average Mass [g]**	**Average Length [mm]**	**Average Remainig Area [mm²]**
NC (reference)		149.4097	188.50	93.00
LP		132.487	169.50	91.71
HDP		119.7671	160.00	87.83
UC		129.3556	183.00	82.94
HC		129.2467	202.75	74.80

Table 5. Steel plates and interface elements properties adopted in the numerical models.

Spring Properties		**Plates Properties**	
K_t [N/mm]	**K_c [N/mm]**	**E [N/mm²]**	**v**
-7.56E+02	7.56E+13	200000	0.2

Table 6. Concrete properties adopted in the numerical models.

	Undamaged	**Damaged**
X [mm]	-	0.645
f_c [MPa]	43.65	12.9
f_{ct} [MPa]	3.25	0.87

Table 7. Reduction of the mechanical properties and *R* factor for different degrees of corrosion.

LEVEL OF CORROSION		$E_s^{'}$ [MPa]	$f_u^{'}$ [MPa]	$\varepsilon_u^{'}$	η_s	$R\ (\eta_s)$
LP		190133	1787.8	0.0391	1.39	1
HDP		175480	1570.4	0.0198	5.56	1
UC		157021	1296.5	0.0083	10.82	0.57
HC		126292	840.5	0.0067	19.57	0.20

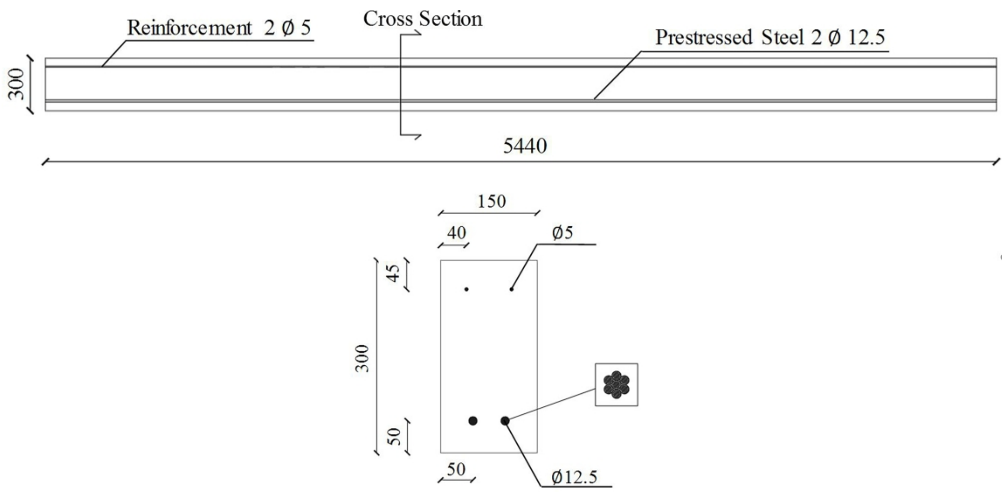

Figure 1. Longitudinal section and cross section of VIGA 470 beam [mm].

438x214mm (300 x 300 DPI)

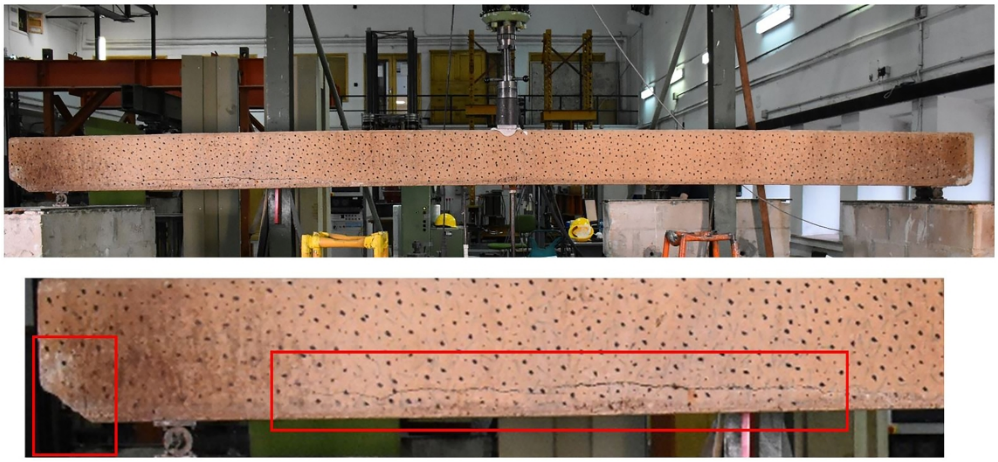

Figure 2. VIGA 470 beam: quantified damage by visual inspection.

420x194mm (300 x 300 DPI)

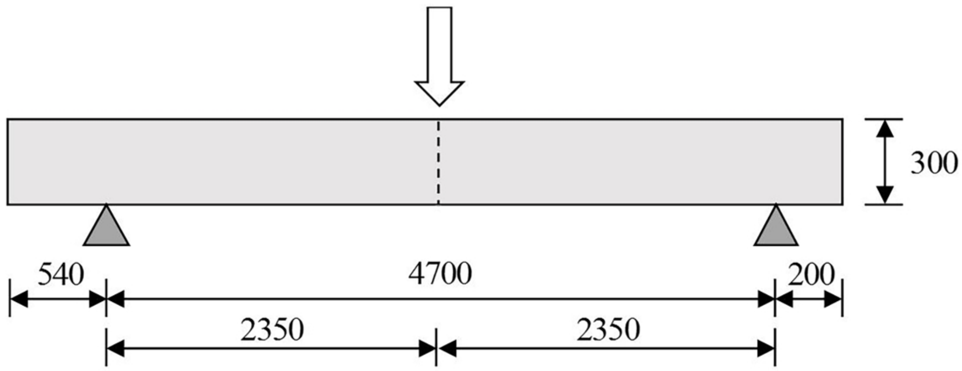

Figure 3. Test setup of VIGA 470 beam.

306x119mm (300 x 300 DPI)

Figure 4. Ultrasound accelerating reaction instrument.

163x151mm (300 x 300 DPI)

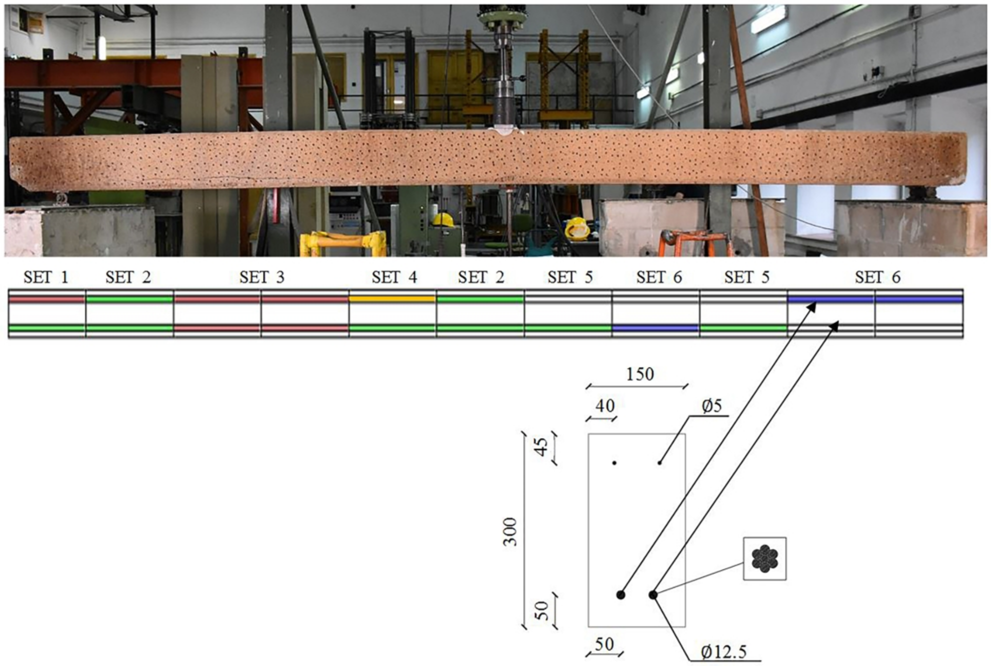

Figure 5. VIGA 470: Correlation between visual inspection and corrosion pattern of the strands.

309x210mm (300 x 300 DPI)

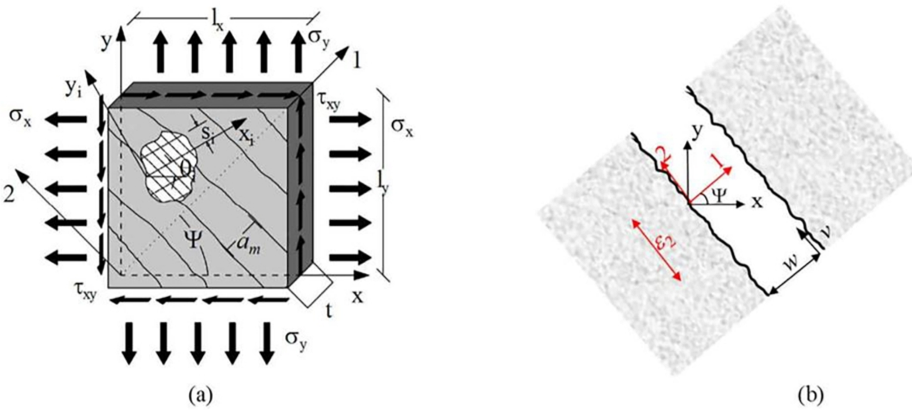

Figure 6. PARC_CL 2.1 crack model: (a) RC membrane element subject to plane stress state, (b) crack parameters.

270x116mm (300 x 300 DPI)

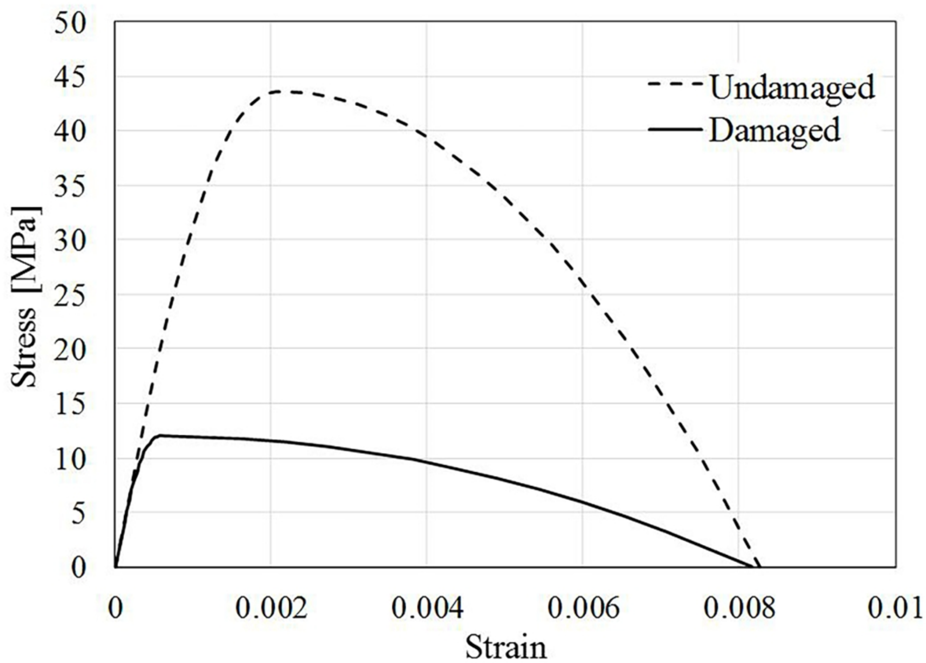

Figure 7. Smeared model and pretension applied to prestressed steel.

230x158mm (300 x 300 DPI)

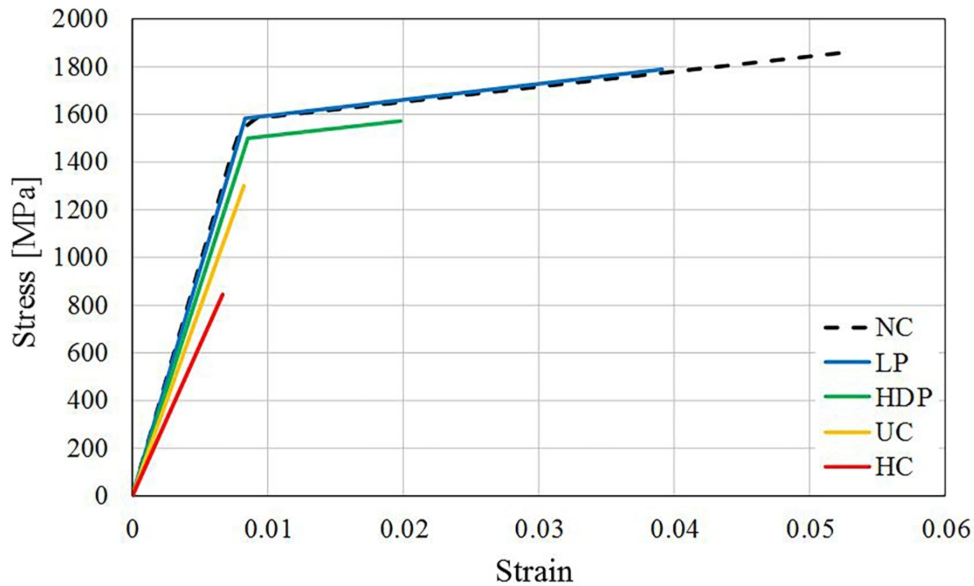

Figure 8. Discrete model and connection between membrane elements and beam elements.

229x143mm (300 x 300 DPI)

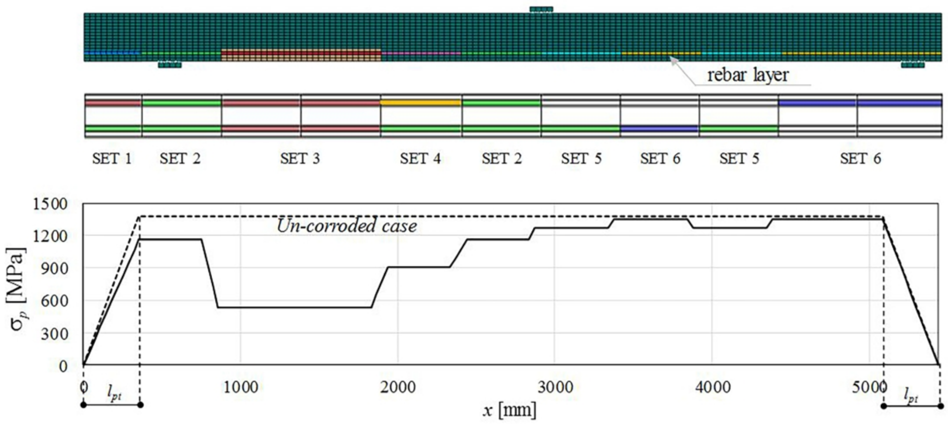

Figure 9. Concrete damage model in compression.

293x130mm (300 x 300 DPI)

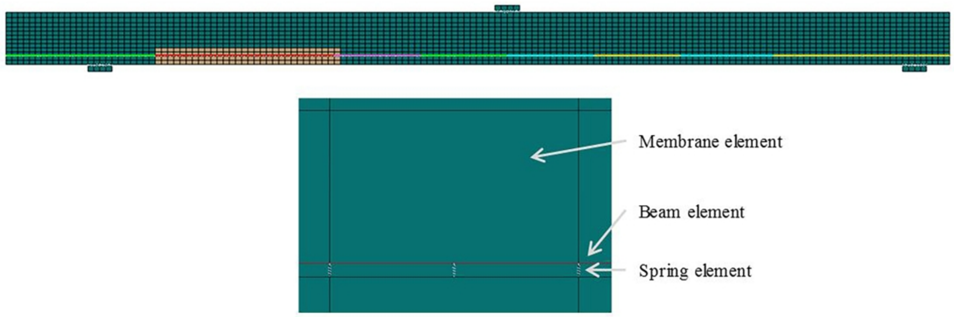

Figure 10. Constitutive model for corroded strands.

300x103mm (300 x 300 DPI)

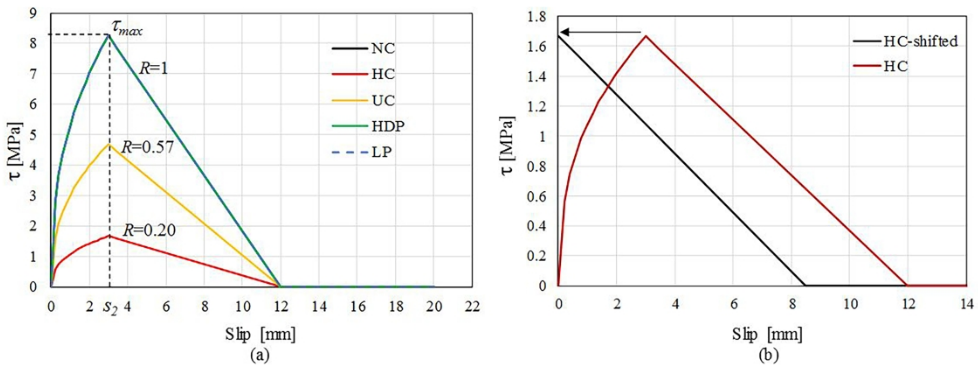

Figure 11. Bond-Slip relationship for splitting failure: (a) deterioration of bond according to Wang et al. (2017) and (b) bond-slip relationship adopted in NLFEA in correspondence of the splitting crack.

308x118mm (300 x 300 DPI)

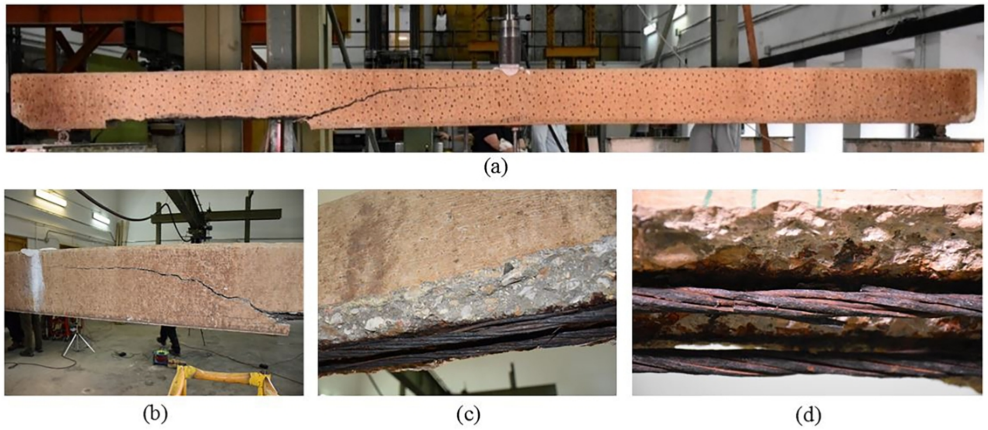

Figure 12. Viga 470 beam at failure: (a) front side, (b) detail of the crack in the back side, (c) and (d) details of corroded strands in correspondence of the concrete cover expulsion.

308x136mm (300 x 300 DPI)

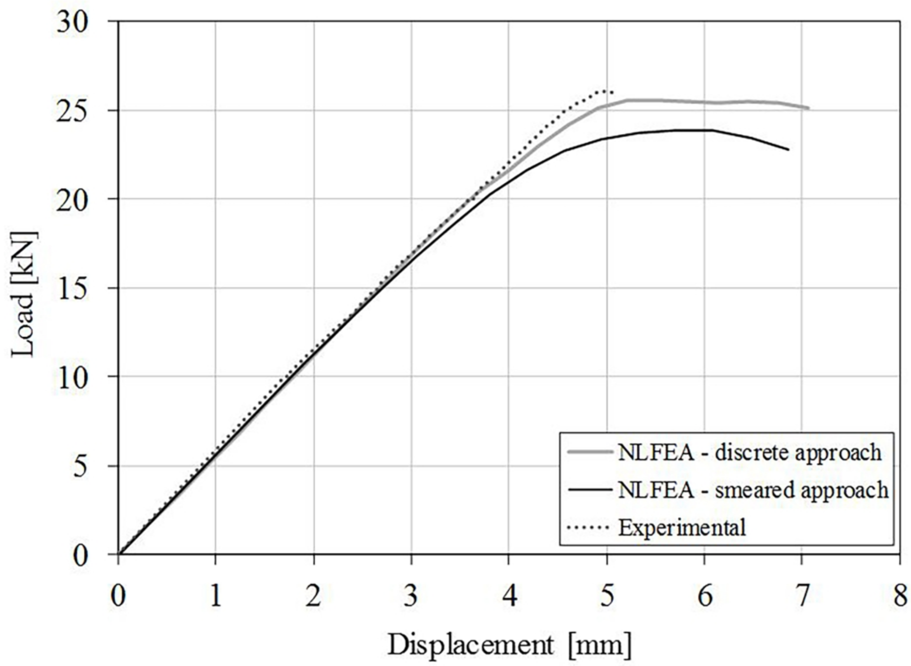

Figure 13. Comparison between experimental and numerical results.

224x156mm (300 x 300 DPI)

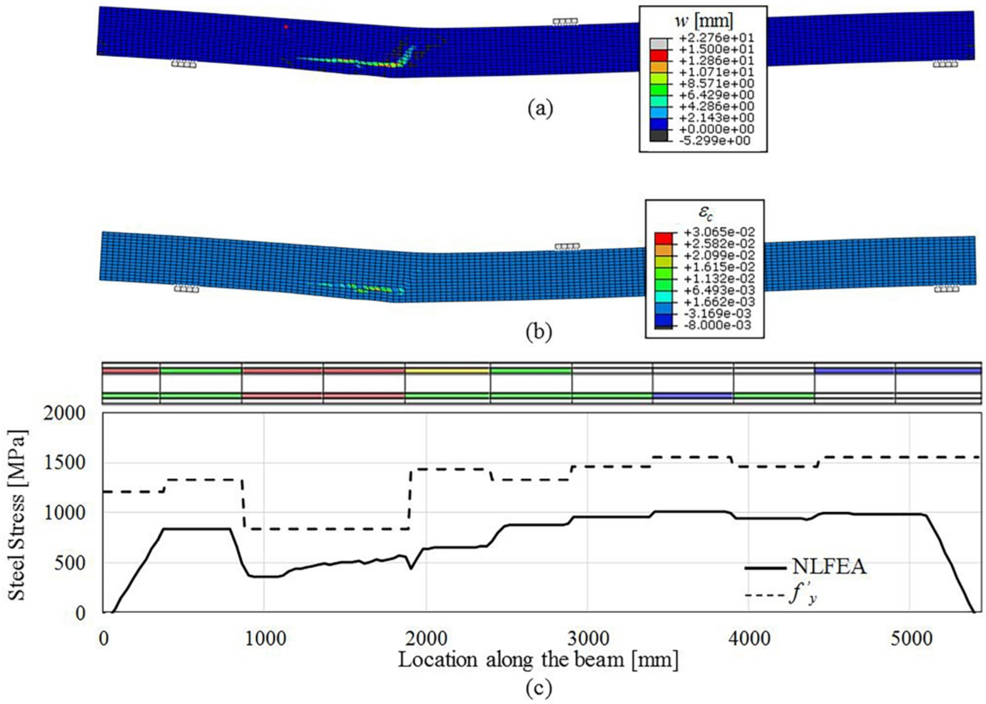

Figure 14. NLFE results at the end of the analysis obtained using the smeared approach: (a) crack width, *w*, (b) concrete strain and (c) strands stresses.

272x198mm (300 x 300 DPI)

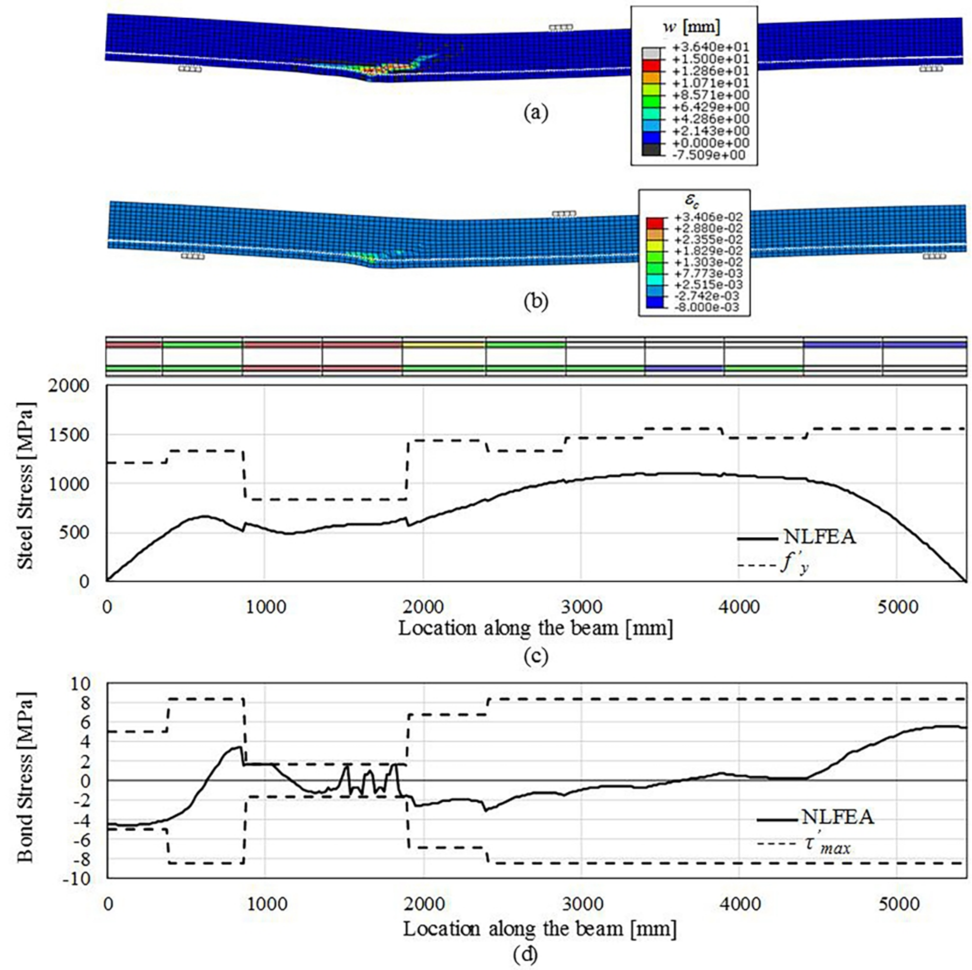

Figure 15. NLFE results at the end of the analysis obtained using the discrete approach: (a) crack width, *w*, (b) concrete strain, (c) strands stresses and (d) bond stresses.

220x213mm (300 x 300 DPI)

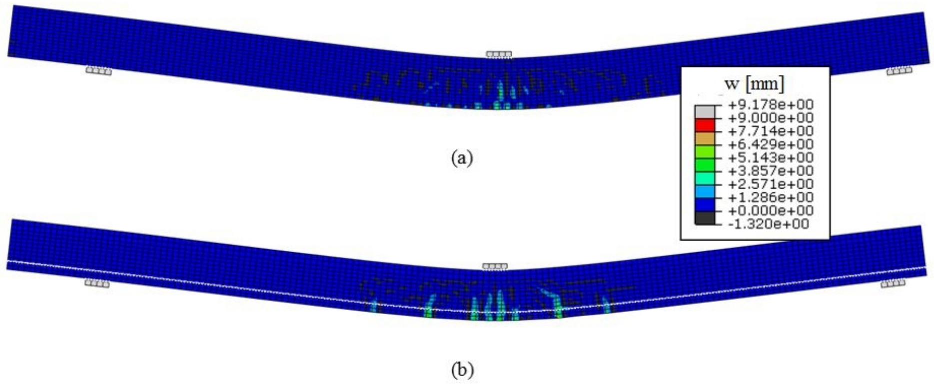

Figure 16. Crack pattern at failure of the uncorroded beam obtained by NLFE analysis: (a) smeared approach and (b) discrete approach.

260x105mm (96 x 96 DPI)

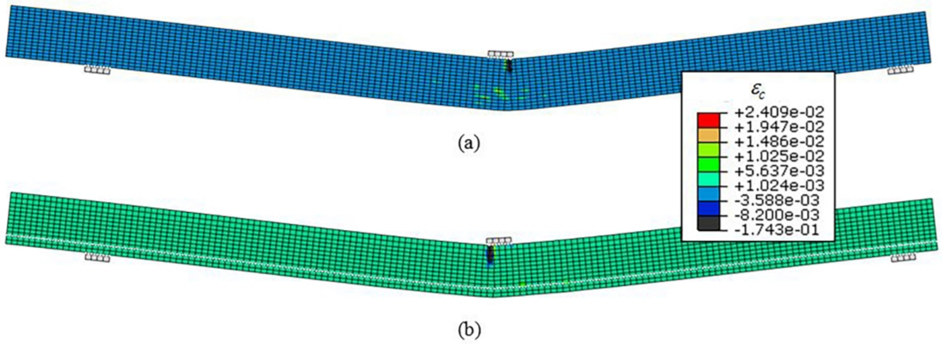

Figure 17. Concrete strain, ε_c, at failure obtained by NLFE analysis of the uncorroded beam: (a) smeared approach and (b) discrete approach.

255x92mm (300 x 300 DPI)

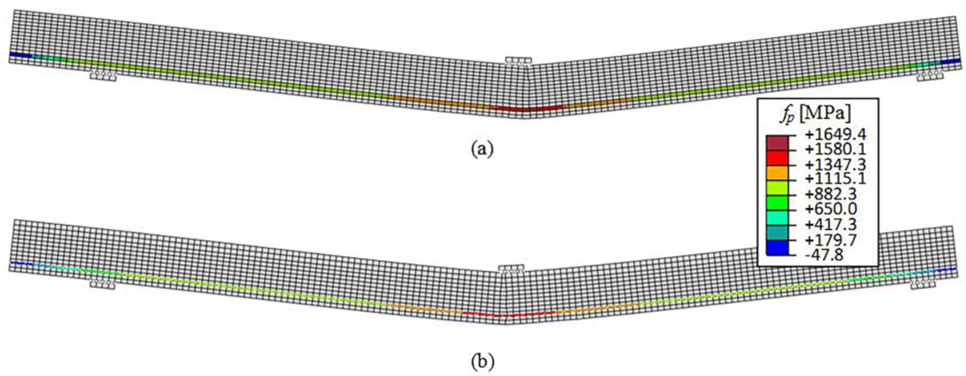

Figure 18. Strands stress, f_p, at failure obtained by NLFE analysis of the uncorroded beam: (a) smeared approach and (b) discrete approach.

251x97mm (300 x 300 DPI)

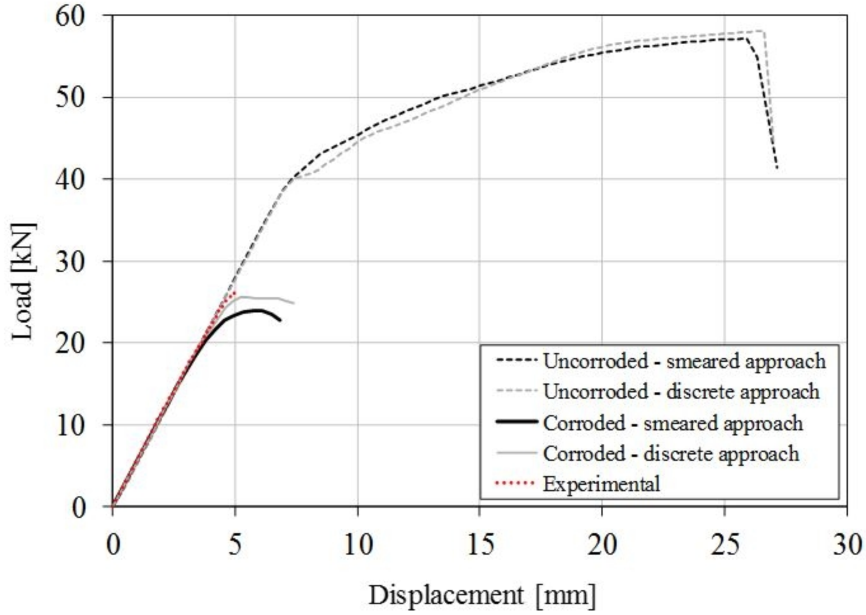

Figure 19. Comparison between experimental and numerical results using uncorroded properties.

208x135mm (96 x 96 DPI)

Reviewer: 1

It is not clear, why only one of eight available beams was investigated. E. g. in Fig. 1 the cross section „of the beams" are specified, but – as far as recognisable – only „VIGA 470" was examined.

The experimental campaign conducted at the Instituto Eduardo Torroja has not yet been published.

Since it is necessary to present the experimental evidences in order to explain the choices of the numerical model, the authors decided to present the model of one beam until the experimental campaign is published. In this paper, a modelling procedure for the analysis of PC and RC elements is proposed and in future it will applied to the whole campaign.

In order not to confuse the reader, the text was modified in paragraph 2.

1. **In this context: What is meant in Fig. 3: „Test setup of VIGA470 beams"? Page 5: VIGA 470/VIGA 470 (inconsistent with and without blank) is „one of eight…"**
   Figure 3 presented a typing error and for this reason the caption was modified with "*Test setup of VIGA 470 beam.*"

2. **In which way the values of Tab. 1 were determined? Meanvalues of 8 beams?**
   f_c is the mean value of the compressive strength of concrete declared by the manufacturer. The tensile strength f_{ct} and the modulus of elasticity E_c were obtained according to fib Model Code 2010.
   $$f_{ctm} = 0.3 \cdot \left(f_{ck}\right)^{2/3}$$
   $$E_{ci} = E_{c0} \cdot \alpha_E \cdot \left(\frac{f_{ck} + \Delta f}{10}\right)^{1/3}$$

3. **„concrete properties of damaged cover" in Tab. 6 are adopted values and should be declared appropriate in the legend**
   According to this remark the caption of Table 6 has been modified with: *"Concrete properties adopted in the numerical models."*

4. **Fig 17: Load-diplacement relation of „Experimental" is (almost) not readable.**
   According to this remark the figure has been modified using different colors.

5. **It schould be mentioned, that the good relation between experiment and assessment and the drawn conclusions are initially valid for one parameter constellation and can not be considered as generally admitted.**
   According to this remark, the conclusions are rewritten.

Reviewer: 2

This paper presents the experimental test and numerical analysis for the prestressed concrete on the corroded environment. Their procedure was quite reasonable and derived meaningful conclusions. However, the experimental test results are insufficiently explained, and there are some differences between the research purpose mentioned in the introduction and conclusions. The authors are requested to revise their manuscript according to the comments outlined below:

The reviewer is thanked for the interesting comments. Your suggestions have allowed to improve the paper as well as the numerical results. For this reason the paper is reorganised and some figures are added in order to better clarify the modelling procedure and numerical results.

1. **What are the failure criteria in the FE analysis and which criterion was governed for the failure? In Figure 13, The FEA results seem to be able to behave to the larger displacement, especially in the discrete approach. The post-peak behavior needs to be shown during the reduction of load.**

   According to this remark the authors try to improve the analysis conducted using the discrete approach. The new result is shown in Figure 15 and Figure 13. After the last increment (shown in Figure 13) both the models (smeared and discrete) shown a slight post peak behaviour. However, due to convergence problems it was not possible to show a marked post peak behaviour. This is due to the achievement of very high values of crack openings (see Figure 14(a) and Figure 15 (a)) linked to the model adopted for the aggregate interlock.
   The NLFEA were conducted using the Newton-Raphson's convergence method that does not permit to fit very well the post-peak behavior. To try reaching convergence it would be better to use the Arc length method, but unfortunately Abaqus does not allow to use this convergence method with user subroutines.

2. **In the material properties of strands, even though the authors used the existing model (Lu et al. 2019) the phenomena of the reduction of strength and ductility need to be explained; why the strands changed to brittle materials, why the elastic modulus changed, etc.**
   It is in the authors opinion that the phenomena related to the corrosion process associated to the experimental campaign of Lu et al. 2019 are well explained in the reference paper. For sake of brevity the authors prefer to refer to the paper and save space for the numerical results. The paragraph associated to this part was rewritten:
   "In previous studies the properties of the corroded reinforcements were studied and it was found out that the stress-strain curve of the corroded steel is affected by the corrosion degree. The ductility and the strength of the residual section decrease. This is recognized in Lu, Li & Zhao (2016) paper who proposed a damage model for failure mechanism of corroded prestressed strands that has been adopted in this paper. In Lu, Li & Zhao (2016) damage model, the following mechanical properties are dependent on corrosion level: the elastic modulus, Equation (6), the ultimate strength of strands (due to the stress concentration caused by pitting corrosion and/or eccentric tension due to asymmetric corrosion distribution), Equation (7), and the ultimate strain, Equation (8). Furthermore, Lu, Li & Zhao (2016) observed that when the corrosion degree is larger than 8% the steel loses the yielding plateau and the strain hardening region."

3. **In the smeared crack model, the authors mentioned the bond between concrete and strands was assumed perfect, but the reviewer wonders how to realize the bond failure as shown in Fig. 12.**
   According to this remark, paragraph 3.3 has been rewritten and additional information about NLFEA results have been added:
   "During the experimental test, the beam showed a sudden brittle failure in correspondence of a load equal to 26 kN, with concrete cover expulsion in correspondence of the splitting crack, Figure 12(a). The beam

at the end of the test showed a shear and bond failure, according to the definition expressed in the CONTECVET [CONTECVET IN30902I, (2001), Figure 12(b). In correspondence of the concrete cover expulsion the strands were highly corroded with some wires broken, Figure 12(c-d). The load-displacement curve is characterized only by the elastic part, losing any ductile behaviour, Figure 13. Figure 14 and Figure 15 show the numerical results obtained using the smeared and the discrete approach respectively. Both the models demonstrate to be able to catch with good approximation the ultimate resistance of the beam. Since the NLFEA have been carried out in displacement control, the numerical ductility results higher than the ductility measured during experimental test carried out in load control. The failure mode obtained using both the approaches is governed by high crack opening width values, Figure 14(a) and Figure 15(a), without crushing of concrete, Figure 14(b) and Figure 15(b). A single crack was formed, characterized by a horizontal part and an inclined part. The formed crack is due to a biaxial state governed by tensile stresses induced by bending and shear stresses induced by shear. The layer of concrete plain elements above the strands is characterized by a different stiffness and strength that increases tangential shear stresses in concrete, causing the formation of the horizontal crack where the mechanical properties of concrete have been degraded due to strands corrosion effects. In Figure 14(c) and Figure 15(c), the strands stresses obtained by NLFEA along the beam are shown for smeared and discrete approach respectively and compared with the yielding stresses associated to each corrosion level: in both the cases, the strands have not reached the yielding stress. In the smeared approach the NLFEA stopped due to the reaching of high value of crack openings in correspondence of the splitting crack, as shown in Figure 14. In the discrete approach, in addition to high crack opening values, the NLFEA shows the reaching of the maximum bond stress in correspondence of the splitting crack, Figure 15(d). "

4. **Please use the SI unit in all paragraphs and figures. i.e., strands diameter in Fig.1, the distance of support to the corners, etc.**

   According to this remark the figures and the dimension of the beam have been modified.

5. **For the visual inspection, were some devices used? If then, please mention them. In addition, the criteria for the classification of the corrosion level need to be mentioned.**

   - Before the test, a visual evaluation of the damages on the beam (as cracks and spalling) was carried out without using any tool:

   "Visual inspection was performed to identify and quantify the damage in the beam in terms of presence of cracks and spalling of concrete cover, highlighting the presence of an extended splitting crack in correspondence of the strands and cover expulsion in the left corner, Figure 2.

   - After the test, the strands were extracted.
   - 5 levels of corrosion were identified from the visual inspection (shown in Table 3): "*In order to analyse the corrosion distribution along the length of the beam, after the test the concrete cover was removed and the strands were extracted. From the visual inspection five levels of corrosion were considered: not corroded (NC), localized pits (LP), high-density pits (HDP), uniform/generalized corrosion (UC), high corrosion (HC), as summarized in Table 3"*
   - Subsequently: "*For each level of corrosion, a sample was selected and measured. In particular, each sample strand was separated into wires and cleaned from the rust using a cleaning solution (which does not affect the parent metal) and the tank instrument with ultrasound energy shown in Figure 4. After the cleaning procedure, the samples were weighed and measured in terms of length, obtaining the mean values reported in Table 4."*
   - The two strands were extracted from the beam and divided in 500 mm long pieces.
   - A level of corrosion was assigned to each piece of strand using the classification reported in Table 3, comparing the photos with the condition of the piece of the strand:

"Subsequently, each strand was divided into 500 mm long pieces which were classified according to the detected level of corrosion defined in Table 4.."

- Finally, the corrosion pattern of the strands was defined: "*By means of this procedure the corrosion distribution along both the strands of VIGA 470 beam was defined, Figure 5."*

6. In Figure 7, the legends which were classified by corroded and uncorroded were inappropriate. The concrete shall be related to the perpendicular strain. In the manuscript and Figure 7, the reduction of compression strength was about 75%, but it was in the tension zone where the concrete capacity was not important. Regarding this, the authors shall mention which concrete model was applied to which part.

(Figure 7 became Figure 9 in the revised manuscript) The legend of Figure 9 has been modified with damaged and undamaged.

The authors agree with the reviewer comment, as the model proposed by Coronelli et al. reduces the properties of concrete in compression. However, as shown in Table 6, the tensile strength f'ct was obtained from the value of the reduced compressive strength f'c. The reduced properties of concrete were assigned to the elements in ocher in Figure 7 and Figure 8. According to this remark the following sentence has been added: "*As consequence, also the tensile strength of concrete has been reduced according to the compressive strength of the damaged concrete,* f'_c*"*.

Furthermore, it is important to remark that the PARC_CL 2.1 crack model considers the biaxial state of concrete. [Belletti, B., Scolari, M., & Vecchi, F. (2017a). PARC_CL 2.0 crack model for NLFEA of reinforced concrete structures under cyclic loadings. Comput Struct, 191(2017), 165-179.]

7. The experimental results were insufficient. If there was another paper that dealt with the experimental results, please provide as the reference. If not, the test results such as the strength, crack pattern, failure mode, and strain shall be added.

It is in the authors' opinion that the behaviour of naturally corroded prestressed beams is a topic that has not yet been fully developed. Furthermore, always in this subject the number of results is insufficient. The authors are based in those made under CONTECVET project which were comparatively the largest set of data available on the performance of corroding structural elements. The exercise made here is a step more in the remaining long path needed to have rigorous analysis of the corroding elements.

With respect to the "strength, crack pattern, failure mode, and strain", the failure mode as well as the crack pattern is shown in Figure 12 and the load-deflection curve of the particular beam in Figure 13. Figure 12 is updated in order to add some information about the condition of the strands and a detail of the crack at the end of the test.

8. The authors mentioned that this paper related to the shear capacity of corroded prestressed beams. However, the reviewer thinks the specimen failed by the bond and it just developed to the shear crack, and even the crushing of concrete around the loading point was not observed. It is very difficult to say that as the shear failure. The crack pattern and failure mode of the specimen shall be analyzed in detail in the experimental study as well as the numerical model.

The authors think that the beam shows a shear failure combined with bond, according to the definition expressed in the CONTECVET [CONTECVET IN30902I, (2001). A validated user's manual for assessing the residual life of concrete structures, DG Enterprise, CEC, (The manual for assessing reinforced structures affected by reinforcement corrosion can be seen at the web sites of IETcc (www.ietcc.csic.es) and GEOCISA (www.geocisa.es))]. The beam reaches the failure in a brittle way:

indeed, the cover expulsion happened suddenly without any warnings. According to this point, the paragraph 3.3 was modified:
"*During the experimental test, the beam showed a sudden brittle failure in correspondence of a load equal to 26 kN, with concrete cover expulsion in correspondence of the splitting crack, Figure 12(a). The beam at the end of the test showed a shear and bond failure, according to the definition expressed in the CONTECVET [CONTECVET IN30902I, (2001), Figure 12(b). In correspondence of the concrete cover expulsion the strands were highly corroded with some wires broken, Figure 12(c-d). The load-displacement curve is characterized only by the elastic part, losing any ductile behaviour, Figure 13.*"

Since the bond-slip relationship proposed by Wang et al. (2017) derived from tests on specimens with strands and transverse reinforcement, the authors modified the bond-stress relationship in Eq.17. In particular the authors modified the residual bond stress τ_f (equal to zero) according to Model Code 2010 for splitting failure and unconfined cases. According to this remark Figure 11 was modified.
"*Since the VIGA 470 was without stirrups, in this paper the residual strength has been assumed to be equal to zero.*"

The beam, before the test, showed an important splitting crack (Figure 5), therefore the authors modified the bond-slip relationship used in the smeared approach:
"*In correspondence of the splitting crack it is reasonable to consider that splitting failure is occurring. For this reason, the local bond stress-slip relationship in correspondence of the splitting crack (i.e. springs placed in correspondence of elements in ocher color in Figure 10) can be approximated by shifting the reference curve in the slip direction, as shown in Figure 11 (b).*

The NLFEA conducted using the discrete approach has been updated according to the modification of the bond-slip relationship. This modification has been permitted to improve the result as shown in Figure 14 and 15.

Finally, pertaining to the above explanation, the following sentence has been added to the conclusions:

"Future developments will be aimed at investigating in more detail the collapse mechanisms of PC structures, in order to validate the proposed modelling strategy and evaluate in which cases the discrete approach is preferable and necessary."

The authors are confident that the proposed numerical approach is suitable for different failure modes. The obtained results for VIGA 470 are encouraging and in future the authors will apply the procedure to the entire experimental campaign in order to demonstrate the validity of the model. Furthermore, in case of VIGA 470, the smeared and the discrete approaches provide similar results. Analyzing other prestressed beams with different test setups and corrosion levels will clarify when one procedure is preferable than the other.

9. The shear span – depth ratio was almost 10 but it seems to be very short for the shear test. Was there any reason with the ratio? Was the design shear strength higher than the shear force at the flexural strength?

From analytical calculation the design shear strength is higher than the shear force at the flexural strength. Since the beam has not constant and uniform properties in its length it was necessary to evaluate the resistance in pre-established sections (the sections have been placed at the center line of each corrosion level shown in Figure 5). Therefore, shear strength Vrd (adopting ModelCode 2010, level II) and flexural strength resistance Mrd have been obtained in function of reduced mechanical properties due to corrosion. Finally, the ratios between Ved/Vrd and Med/Mrd have been evaluated for each section, as the applied load increases. In this way, the authors obtained that the failure happened due to shear, with an applied load equal to 43.50 kN (while the bending failure happened for an applied load equal to 51.50 kN).